JOC Articles

Supramolecular Assemblies and Redox Modulation of Pyromellitic Diimide-Based Cyclophane via Noncovalent Interactions with Naphthol[1]

Shin-ichiro Kato,[†,‡] Taisuke Matsumoto,[§] Keiko Ideta,[§] Toshiaki Shimasaki,[†,‡] Kenta Goto,[†] and Teruo Shinmyozu*[,†]

Institute for Materials Chemistry and Engineering (IMCE) and Department of Molecular Chemistry, Graduate School of Sciences, Kyushu University, 6-10-1 Higashi-ku, Fukuoka 812-8581, Japan, and Institute for Materials Chemistry and Engineering (IMCE), 6-1 Kasuga-koh-en, Kasuga 816-8580, Japan

shinmyo@ms.ifoc.kyushu-u.ac.jp

Received December 30, 2005

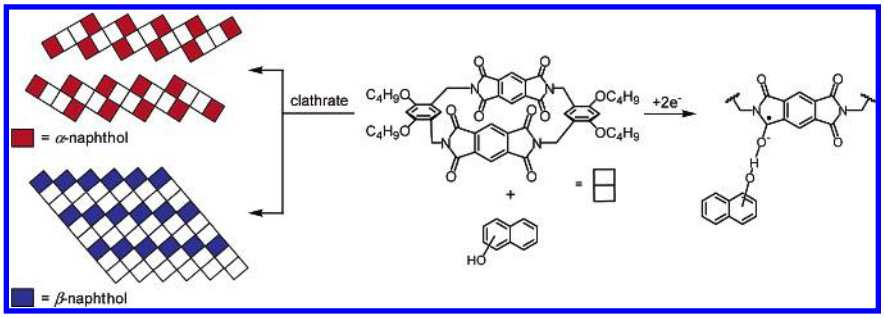

This paper reports the electroscopic and electrochemical properties of [2 + 2] pyromellitic diimide-based cyclophane **1** as well as acyclic *N*,*N*′-bis(2-methoxybenzyl)pyromellitic diimide **2** and the clathrate compounds formed by **1**. Compound **1** was synthesized by direct cyclocondensation. Its structure was determined by an X-ray crystallographic analysis of a single crystal obtained by recrystallization from DMF. The intramolecular charge-transfer interactions of **1** and **2** were characterized by UV/vis spectroscopy and MO calculations. The UV/vis spectra showed that the tail of a longer wavelength absorption of both **1** and **2** reached the visible region. MO calculations (B3LYP/6-31G*) showed that the HOMO and LUMO orbitals of **1** and **2** substantially localize in the xylyl and pyromellitic diimide moieties across the methylene linker, respectively. The X-ray crystallographic analyses demonstrated that single crystals grown from a mixture of **1** and α-naphthol and a mixture of **1** and β-naphthol were the clathrate compounds with 1D and 2D supramolecular assemblies, respectively, which are formed by a combination of hydrogen-bonding and charge-transfer interactions. From the cyclic voltammetry measurements, both **1** and **2** showed reversible reduction processes, and the reduction potential observed at −1.09 V vs Ag/Ag^+ for **2** split into two potentials at −1.01 and −1.14 V for **1**. The addition of α- and β-naphthol induced a decrease in the potentials due to the diradical anion of **1** and radical anion of **2** by about 80 mV, and their reduction processes were reversible.

1. Introduction

In the field of supramolecular chemistry, there has been much interest over the past two decades in the design of molecular receptors and mechanically interlocked molecules. For example, catenanes and rotaxanes, and nanoscale supramolecular assemblies, have led to the exploitation of many types of intermolecular interactions, including hydrogen bonding,[2] the solvophovic effect,[3] metal−ligand coordination,[4] and charge-

* To whom correspondence should be addressed. Tel: +81 92 642 2716. Fax: +81 92 642 2735.
† Institute for Materials Chemistry and Engineering (IMCE), Kyushu University.
‡ Department of Molecular Chemistry, Kyushu University.
§ Institute for Materials Chemistry and Engineering (IMCE).

(1) Molecular Tubes and Capsules. 2. For part 1, see: Iwanaga, T.; Nakamoto, R.; Yasutake, M.; Takemura, H.; Sako, K.; Shinmyozu, T. *Angew. Chem., Int. Ed.* **2006**, *45*, 3643−3647.

10.1021/jo0600196 CCC: $33.50
Published on Web 05/27/2006

transfer (CT) interaction.[5] In the CT interaction, aromatic diimide-based macrocycles with a strong electron-withdrawing properties have been widely used for the creation of the above supramolecular structures[1,6−9] and investigation of transannular interactions.[10−12] For example, the construction of aromatic-diimide based macrocycles is a key synthetic procedure for various neutral [2]catenanes by taking advantage of the CT interaction between the electron-rich aromatic host and an included electron-deficient aromatic diimide derivatives as a guest.[7,8] New supramolecular assemblies such as [3]pseudo-rotaxane[13] and macrocycle−tweezer complexes[14] have been successfully synthesized by using this methodology. The aromatic diimide-based macrocycles with a planar chirality have recently been reported.[15] Lately, we have reported the first example of "cyclophanes within cyclophanes" that has been confirmed by X-ray crystallography and whose driving force is a CT interaction between an aromatic diimide and a benzene ring.[1] The created supramolecular structures would be considered as attractive functional materials due to the presence of photophysically and electrochemically active aromatic diimides.[16,17] Therefore, it is important to understand the nature of the relationship between the activities and molecular structures of aromatic diimide-based macrocycles as structural components for supramolecular structures. Furthermore, aromatic diimides, whose conformation is controlled by 2-*tert*-butylphenyl groups at the nitrogen atoms, have been reported to form sandwich-like clathrate compounds and a 2D network by a combination of CT interactions, CH−π interactions, and hydrogen bonding.[18]

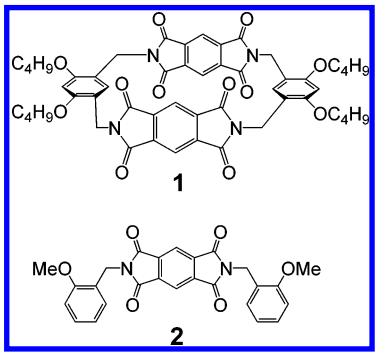

FIGURE 1. Structures of [2 + 2] pyromellitic diimide-based cyclophane **1** and acyclic pyromellitic dimide derivative **2**.

In this context, our interest in the electroscopic and electrochemical properties of the aromatic diimide-based macrocycles and their formation of new-type supramolecular assemblies via noncovalent interactions led us to design and synthesize the simple [2 + 2] pyromellitic diimide-based cyclophane **1** (Figure 1). The high solubility in common organic solvents due to the attachment of butoxy groups to the benzene unit should allow the investigation of the electroscopic and electrochemical properties under various solution conditions, and the introduction of a methylene linker between the pyromellitic diimide moiety and the benzene unit should leave the sufficient electron-withdrawing property to the pyromellitic diimide moiety for the formation of supramolecular assemblies. We now report here the synthesis and structural properties of **1** and its electroscopic and electrochemical properties with the acyclic *N*,*N*′-bis(2-methoxybenzyl)pyromellitic diimide **2** as a reference. We will then describe the formation of clathrate compounds formed of **1** with naphthols and their electroscopic and electrochemical properties based on the UV/vis spectra, MO calculations, cyclic voltammograms, and X-ray crystallographic analyses. Finally, the redox modulation of **1** and **2** via noncovalent interactions with naphthols will be demonstrated in cyclic voltammetry measurements.

(2) For reviews of hydrogen-bonded assemblies, see: (a) Conn, M. M.; Rebek, J., Jr. *Chem. Rev.* **1997**, *97*, 1647−1668. (b) Rebek, J., Jr. *Acc. Chem. Res.* **1999**, *32*, 278−286. (c) Rebek, J., Jr. *Chem. Commun.* **2000**, 637−643. (d) Greig, L. M.; Philp, D. *Chem. Soc. Rev.* **2001**, *30*, 287−302. (e) Prins, L. J.; Reinhoudt, D. N.; Timmerman, P. *Angew. Chem., Int. Ed.* **2001**, *40*, 2382−2426.

(3) Cubberley, M. S.; Iverson, B. L. *J. Am. Chem. Soc.* **2001**, *123*, 7560−7563 and references therein.

(4) For reviews of metal-coordinative assemblies, see: (a) Fujita, M. *Chem. Soc. Rev.* **1998**, *27*, 417−425. (b) Caulder, D. L.; Raymond, K. N. *Acc. Chem. Res.* **1999**, *32*, 975−982. (c) Caulder, D. L.; Raymond, K. N. *J. Chem. Soc., Dalton Trans.* **1999**, 1185−1200. (d) Seidel, S. R.; Stang, P. J. *Acc. Chem. Rec.* **2002**, *35*, 972−983. (e) Vilar, R. *Angew. Chem., Int. Ed.* **2003**, *42*, 1460−1477. (f) Fujita, M.; Tominaga, M.; Hori, A.; Therrien, B. *Acc. Chem. Res.* **2005**, *38*, 371−380.

(5) For reviews of aromatic interactions, see: (a) Hunter, C. A.; Lawson, K. R.; Perkins, J.; Urch, C. J. *J. Chem Soc., Perkin Trans. 2* **2001**, 651−669. (b) Meyer, E. A.; Castellano, R. K.; Diederich, F. *Angew. Chem., Int. Ed.* **2003**, *42*, 1210−1250. (c) Klärner, F.-G.; Kahlert, B. *Acc, Chem. Res.* **2003**, *36*, 919−932. (d) Zhao, D.; Moore, J. S. *Chem. Commun.* **2003**, 807−818.

(6) For molecular receptors, see: (a) Jazwinski, J.; Blacker, A. J.; Lehn, J.-M.; Cesario, M.; Guilhem, J.; Pascard, C. *Tetrahedron Lett.* **1987**, *28*, 6057−6060. (b) Anderson, H. L.; Hunter, C. A.; Meah, M. N.; Sanders, J. K. M. *J. Am. Chem. Soc.* **1990**, *112*, 5780−5789. (c) Bilyk, A.; Harding, M. M. *Chem. Commun.* **1995**, 1697−1698. (d) Houghton, M. A.; Bilyk, A.; Harding, M. M.; Turner, P.; Hambley, T. W. *J. Chem. Soc., Dalton. Trans.* **1997**, 2725−2733. (e) Chen, G.; Lean, J. T.; Alcalá, M.; Mallouk, T. E. *J. Org. Chem.* **2001**, *66*, 3027−3034.

(7) For review of catenanes and oligocatenanes, see: Raehm, L.; Hamilton, D. G.; Sanders, J. K. M. *Synlett* **2002**, 1743−1761.

(8) For neutral [2]catenanes, see: (a) Hamilton, D. G.; Sanders, J. K. M.; Davies, J. E.; Clegg, W.; Teat, S. J. *Chem. Commun.* **1997**, 897−898. (b) Hamilton, D. G.; Davies, J. E.; Prodi, L.; Sanders, J. K. M. *Chem. Eur. J.* **1998**, *4*, 608−620. (c) Zhang, Q.; Hamilton, D. G.; Feeder, N.; Teat, S. J.; Goodman, J. M.; Sanders, J. K. M. *New. J. Chem.* **1999**, *23*, 897−903. (d) Hamilton, D. G.; Prodi, L.; Feeder, N.; Sanders, J. K. M. *J. Chem. Soc., Perkin Trans. 1* **1999**, 1057−1065. (e) Hamilton, D. G.; Montalti, M.; Prodi, L.; Fontani, M.; Zanello, P.; Sanders, J. K. M. *Chem. Eur. J.* **2000**, *6*, 608−617. (f) Hansen, J. G.; Feeder, N.; Hamilton, D. G.; Gunter, M. J.; Becher, J.; Sanders, J. K. M. *Org. Lett.* **2000**, *2*, 449−452. (g) Gunter, M. J.; Farquhar, S. M. *Org. Biomol. Chem.* **2003**, *1*, 3450−3457. (h) Fallon, G. D.; Lee, M. A.-P.; Langford, S. J.; Nichols, P. J. *Org. Lett.* **2004**, *6*, 655−658.

(9) For [2]rotaxanes, see: (a) Nakamura, Y.; Minami, S.; Iizuka, K.; Nishimura, J. *Angew. Chem., Int. Ed.* **2003**, *42*, 3158−3162. (b) Wang, X.-Z.; Li, X.-Q.; Shao, X.-B.; Zhao, X.; Deng, P.; Jiang, X.-K.; Li, Z.-T.; Chen, Y.-Q. *Chem. Eur. J.* **2003**, *9*, 2904−2913. (c) Iijima, T.; Vignon, S. A.; Tseng, H.-R.; Jarrosson, T.; Sanders, J. K. M.; Marchioni, F.; Venturi, M.; Apostoli, E.; Balzani, V.; Stoddart, J. F. *Chem. Eur. J.* **2004**, *10*, 6375−6392.

(10) Borkent, J. H.; Verhoeven, J. W.; de Boer, Th. J. *Chem. Phys. Lett.* **1976**, *42*, 50−53.

(11) Staab, H. A.; Nikolic, S.; Krieger, C. *Eur. J. Org. Chem.* **1999**, 1459−1470.

(12) Hansen, J. G.; Bang, K. S.; Thorup, N.; Becher, J. *Eur. J. Org. Chem.* **2000**, 2135−2144.

(13) Colquhoun, H. M.; Williams, D. J.; Zhu, Z. *J. Am. Chem. Soc.* **2002**, *124*, 13346−13347.

(14) (a) Colquhoun, H. M.; Zhu, Z.; Williams, D. J. *Org. Lett.* **2003**, *5*, 4353−4356. (b) Colquhoun, H. M.; Zhu, Z. *Angew. Chem., Int. Ed.* **2004**, *43*, 5040−5045.

(15) Degenhardt, C. F., III; Smith, M. D.; Shimizu, K. D. *Org. Lett.* **2002**, *4*, 723−726.

(16) For review of perylene bisimide dyes, see: Würthner, F. *Chem. Commun.* **2004**, 1564−1579.

(17) (a) Würthner, F.; Sautter, A.; Schmid, D.; Weber, P. J. A. *Chem. Eur. J.* **2001**, *7*, 894−902. (b) You, C.-C.; Würthner, F. *J. Am. Chem. Soc.* **2003**, *125*, 9716−9725. (c) Würthner, F.; Sautter, A. *Org. Biomol. Chem.* **2003**, *1*, 240−243.

(18) (a) Kishikawa, K.; Tsubokura, S.; Kohmoto, S.; Yamamoto, M.; Yamaguchi, K. *J. Org. Chem.* **1999**, *64*, 7568−7578. (b) Kishikawa, K.; Iwashima, C.; Kohmoto, S.; Yamaguchi, K.; Yamamoto, M. *J. Chem. Soc., Perkin Trans. 1* **2000**, 2217−2221.

SCHEME 1. Synthesis of [2 + 2] Pyromellitic Diimide-Based Cyclophane 1 and Acyclic Pyromellitic Dimide Derivative 2 as a Reference

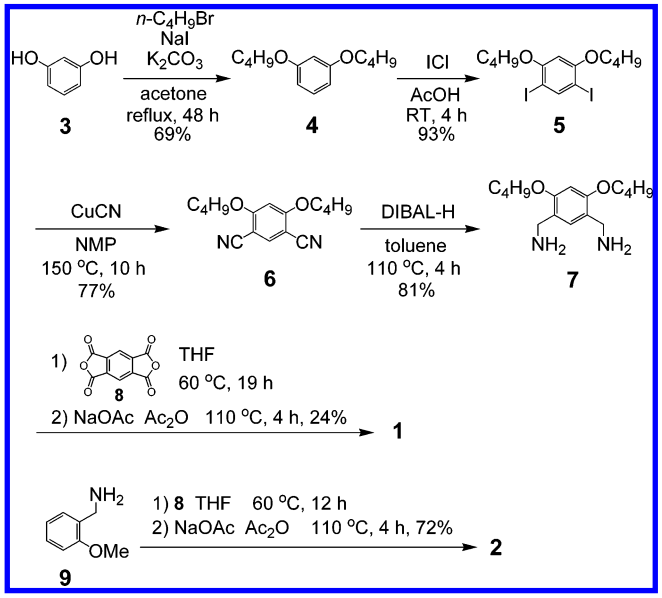

2. Results and Discussion

Synthesis. The synthesis of [2 + 2] pyromellitic diimide-based cyclophane **1** was achieved by means of the direct cyclocondensation of 1,3-bis(aminomethyl)-4,6-di-*n*-butoxybenzene **7** with pyromellitic dianhydride **8** (Scheme 1). The key synthetic intermediate **7** was prepared from resorcinol **3** via four steps (Williamson ether synthesis, iodination, cyanation, and reduction) in about 40% overall yield by optimization of the synthetic procedures reported by Tobe et al.[19] The reduction of 1,3-di-*n*-butoxy-4,6-dicyanobenzene **6** was accomplished by the treatment of diisobutylaluminum hydride at 110 °C in 81% yield to afford the diamine **7**. The direct cyclocondensation of the diamine **7** with the dianhydride **8** in dry THF at 60 °C gave an amic acid,[18a] which was dehydrated to give **1** by treatment with Ac_2O and NaOAc in 24% yield. The formation of the intermediary amic acids were supported by the presence of the broad signals due to the carboxylic acid protons at ca. 13−14 ppm in the ^{1}H NMR spectrum in DMSO-d_6. This coupling reaction exclusively gave the [2 + 2] product **1** and the higher oligomers such as [3 + 3] and [4 + 4] type macrocycles were not isolated. In consequence, **1** was easily purified by conventional column chromatography on silica gel with $CHCl_3$. To estimate the effect of the cyclophane moiety on electroscopic and electrochemical properties, acyclic model compound *N*,*N*′-bis(2-methoxybenzyl)pyromellitic diimide **2** as a reference was prepared from **8** and 2-methoxybenzylamine **9** in 72% yield according to similar procedures for the synthesis of **1**. Compounds **1** and **2** have been fully characterized by spectroscopy and elemental analysis. The molecular structure of **1** has been finally determined by an X-ray crystallographic analysis as described below.

Compound **1** is soluble in $CHCl_3$ and DMF. When it was recrystallized from $CHCl_3$ by vapor diffusion with hexane, pale green needles were obtained, but they gradually effloresced. Single crystals suitable for an X-ray crystallographic analysis were obtained by recrystallization from DMF over 1 week as a clathrate with DMF having the 1:2 stoichiometry. Figure 2 shows the molecular structure of **1** with the selected bond lengths and angles. Transannular pyromellitic diimide π-faces of **1** set in parallel across the xylyl moiety (Figure 2a) with the average transannular distance between the central six-membered rings being 5.06 Å, suggesting very weak transannular π−electronic interactions between them. The distance between C17 and C17* was 9.67 Å. Two xylyl π-faces were almost coplanar but slanted with the distance of only 1.17 Å across the pyromellitic diimide moiety (Figure 2b). The dihedral angle between the pyromellitic diimide π-face and the xylyl π-face was almost perpendicular (85.4°). In **1**·$(DMF)_2$, the DMF molecules served as an adhesive that bound the diimide molecules to form the 1D network aligning the *a*-axis (Figure 3). The DMF molecule not only interacted with the one imide ring of the diimide **1** but also with the carbonyl oxygen of the diimide moiety of the neighboring cyclophane via noncovalent multipoint interactions.

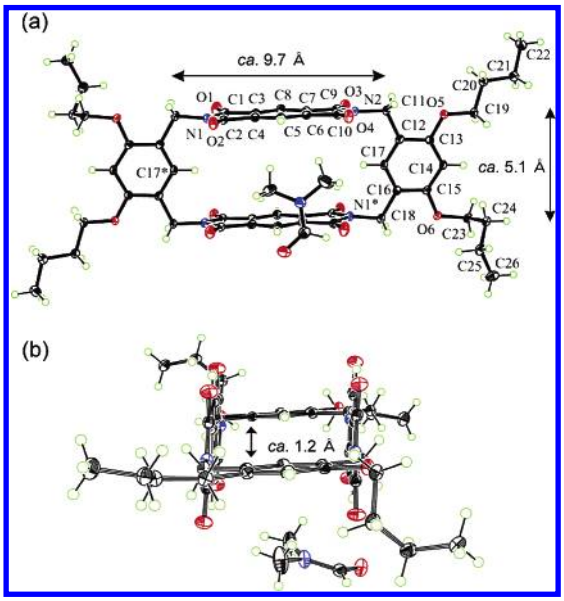

FIGURE 2. ORTEP drawings of the clathrate compound between the pyromellitic diimide-based cyclophane **1** and DMF (1:2): (a) side view; (b) bird's-eye view. Selected bond lengths (Å) and angles (deg): C1−C3 1.499(2), C2−C4 1.496(2), C3−C4 1.391(2), C4−C5 1.384(2), C5−C6 1.388(2), C6−C7 1.394(2), C6−C10 1.495(2), C7−C8 1.383(2), C7−C9 1.496(2), C11−C12 1.515(2), C16−C18 1.511(2), O1−C1 1.204(2), O2−C2 1.206(2), O3−C9 1.206(2), O4−C10 1.203(2), N1−C1 1.391(2), N1−C2 1.390(2), N1*−C18 1.462(2), N2−C9 1.394(2), N2−C10 1.392(2), N2−C11 1.454(2), N2−C11−C12 113.4(1), N1*−C18−C16 114.2(1).

In addition to the *parallel*-conformer observed in the solid state as described above (Figure 2), the *syn*- and *anti*-conformers in **1** may be considered as stable conformational isomers (Figure 4). The temperature-dependent ^{1}H NMR spectrum of **1** in CD_2Cl_2 displayed slight shifts and a broadening of some signals, but no coalescence of the signals due to the stable conformers was observed down to 173 K (Figure S1, Supporting Information), indicating that the cyclophane **1** was quite flexible. To estimate the relative stability of the possible three conformers of **1**, we examined the MO calculations for the cyclophane **1**′, in which the butoxy groups were replaced with methoxy groups in **1** (Figure 5). The B3LYP/6-31G* level of MO calculations predicted that *syn*-**1**′ was the most stable and the *parallel*-**1**′ and *anti*-**1**′ were less stable by 0.5 and 1.1 kcal/mol, respectively.[20] In the solid state, crystal packing forces may contribute to the further stability of the *parallel*-conformers.

(19) Sasaki, S.; Mizuno, M.; Naemura, K.; Tobe, Y. *J. Org. Chem.* **2000**, *65*, 275−283.

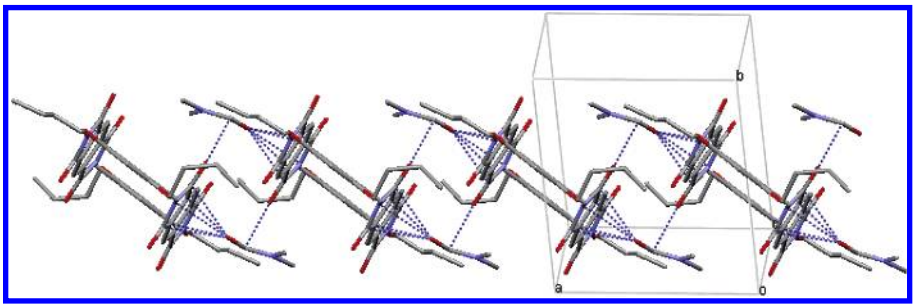

FIGURE 3. 1D molecular arrangement aligning *a*-axis formed in **1**·$(DMF)_2$. Dashed lines are within the sum of the van der Waals radius. Hydrogen atoms are omitted for clarify.

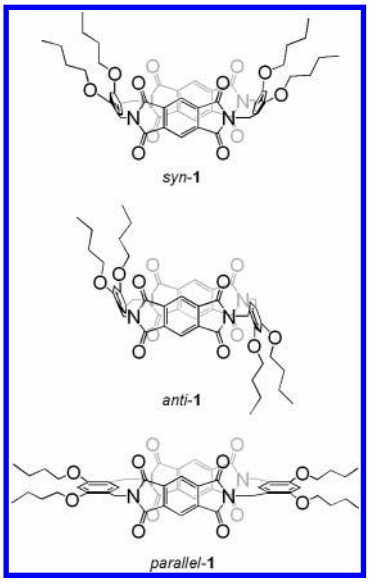

FIGURE 4. Stable conformers of the cyclophane **1**.

UV/vis Spectra. Figure 6a shows the UV/vis spectra of **1** and **2** in $CHCl_3$. The cyclophanes **1** [285 (ϵ 10600), 305 (ϵ 5400), and 317 nm (ϵ 4500)] and **2** [274 (ϵ 7300), 310 (ϵ 2300), and 320 nm (ϵ 2500)] exhibited similar spectra with three absorption maxima (λ_{max}) over 250 nm due to the pyromellitic diimide and alkoxy-substituted benzene chromophores. The bands of **1** and **2** at around 305−310 nm and 317−320 nm were assigned to the short and long axis polarized $\pi-\pi^*$ transitions at the pyromellitic diimide moiety, respectively.[21] The relative intensities of these two bands of **2** were changed when compared with the corresponding bands of **1**. The absorption coefficients (ϵ) (2500) ascribed to a long axis polarized $\pi-\pi^*$ transition was slightly higher than that (2300) of the short axis polarized $\pi-\pi^*$ transition in **2**, whereas the intensity (ϵ 4500) ascribed to a long axis polarized $\pi-\pi^*$ transition was lower than that of the short axis polarized $\pi-\pi^*$ transition (ϵ 5400) in **1**. The magnified figure of the UV/vis spectra over 350 nm of **1** and **2** showed that the tail of the longer absorption band in **1** (Figure 6b), which included an out-of-plane polarized n−π^* transition (340−360 nm),[21] reached the visible region (>400 nm).

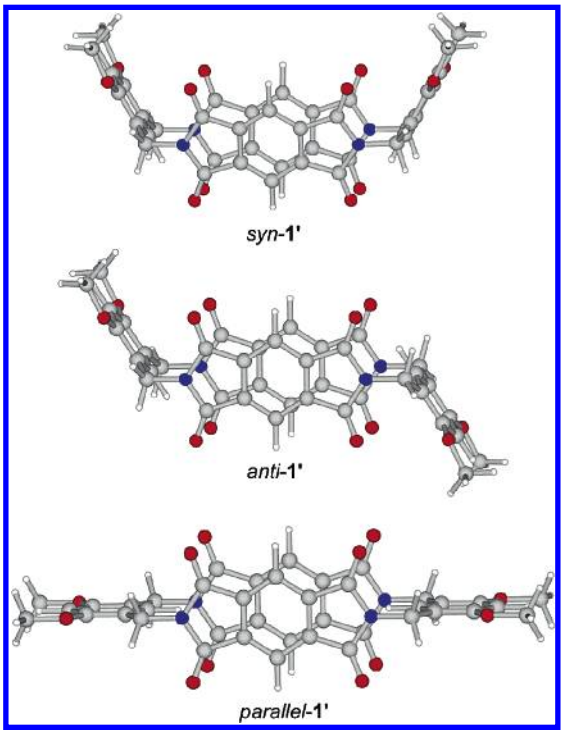

FIGURE 5. Optimized structures of **1′** by MO calculations (Gaussian 03, B3LYP/6-31G*).

Similarly, in the UV/vis spectrum of **2**, the longer absorption band was broad and its tail reached near the visible region analogous to **1**. These probably involved a weak intramolecular CT character from the electron-donating alkoxy-substituted benzene to the electron-withdrawing pyromellitic diimide moiety. The intramolecular CT character was supported by MO calculations (B3LYP/6-31G*) which showed the HOMO and LUMO orbitals of **1** and **2** to be substantially localized in the benzene and pyromellitic diimide moieties, respectively, across the methylene linker (Figure 7). Furthermore, the longer intramolecular CT band of **1** compared to that of **2** was predicted by the calculations (Δ HOMO−LUMO). As a result, the $CHCl_3$ solution of both **1** and **2** as well as in the solid state showed a slight green-yellow color.

Complexation Studies. The finding that the clathrate **1**·$(DMF)_2$ formed a 1D network led us to construct a new supramolecular assembly based on **1** as the clathrate host. We considered that the pyromellitic diimide moiety of **1** should serve as an electron acceptor because the intramolecular CT character was quite weak. To investigate the CT complexation of the electron-poor host **1** and donor guests, the UV/vis spectra of **1** in the presence of various electron-rich aromatic guests were

(20) Optimization of the structures of *syn*-**1′**, *anti*-**1′**, and *parallel*-**1′** conformers was performed by the MO calculations of B3LYP/6-31G* level of theory, and the sum of electronic and zero-point energies was calculated to be −1670584.863 (*syn*-**1′**), −1670583.752 (*anti*-**1′**), and −1670584.247 (*parallel*-**1′**) kcal/mol (Tables S1−S3, Supporting Information).

(21) Gawroński, J.; Brzostowska, M.; Gawrońska, K.; Koput, J.; Rychlewska, U.; Skowronek, P.; Nordén. B. *Chem. Eur. J.* **2002**, *8*, 2484−2494.

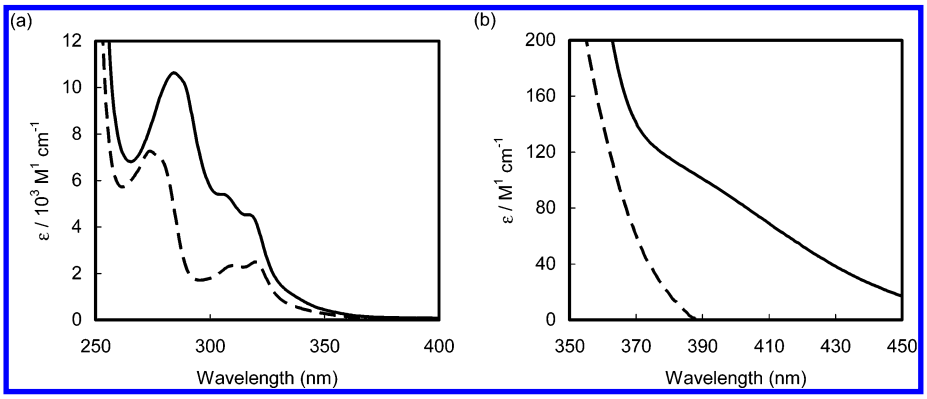

FIGURE 6. (a) UV/vis absorption spectra of **1** (solid line) and **2** (dashed line) in $CHCl_3$ at 1×10^{-4} and 2×10^{-4} M, respectively. (b) Magnified figure around 350−450 nm.

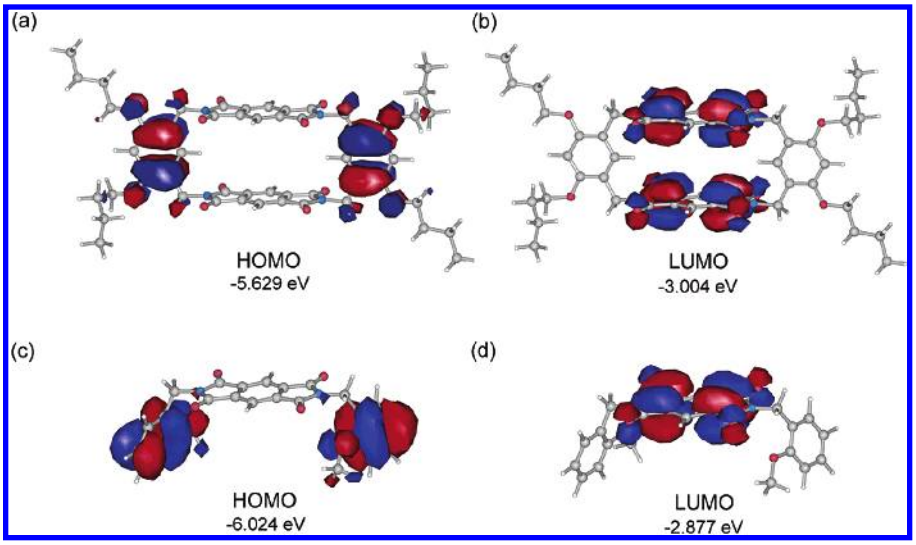

FIGURE 7. (a) HOMO and (b) LUMO orbitals of **1** and (c) HOMO and (d) LUMO orbitals of **2** calculated using the B3LYP/6-31G* level of theory.

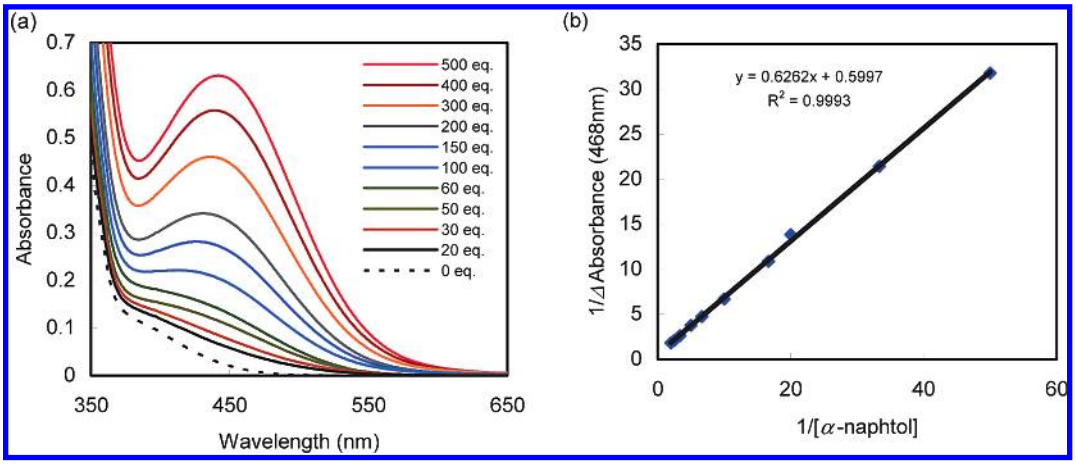

FIGURE 8. (a) Absorption spectra of **1** in $CHCl_3$ at 1×10^{-3} M in the presence of 0−500 equiv of α-naphthol. (b) Benesi−Hildebrand plot.

measured in the concentrated $CHCl_3$ solution (**1**: 1.0×10^{-3} M). As electron-rich aromatic guests, α-naphthol, *β*-naphthol, indole, *p*-dimethoxybenzene, and *p*-xylene were used. Additional CT bands should appear in the intermolecular CT complex between **1** as an acceptor and a donor guest. In the case of α-naphthol, *β*-naphthol, indole, and *p*-dimethoxybenzene, the addition of an excessive amount of the guest to **1** provided the new absorption band in the visible region, which was assigned to the CT band from electron-rich aromatic guests to **1**. For example, the UV/vis spectral changes in Figure 8a typically showed the monotonic growth of the diagnostic CT absorbance upon the incremental addition of α-naphthol to a solution of **1** at 25 °C. The appearance of new CT bands indicated the CT complex formation between **1** and α-naphthol, *β*-naphthol,

TABLE 1. Charge-Transfer Association and HOMO/LUMO Energy Levels of 1 and Guests[a]

compd	K_{CT}[b]	HOMO (eV)	LUMO (eV)
1		−5.629	−3.004
α-naphthol	1.0	−5.464	−0.653
β-naphthol	0.4	−5.543	−0.789
indole	1.0	−5.398	−0.653
p-dimethoxybenzene	0.3	−5.230	+0.086
p-xylene		−6.139	+0.195

[a] HOMO and LUMO energy levels were calculated using the B3LYP/6-31G* level of theory. [b] In $CHCl_3$ containing 1 mM **1** and 20−3000 mM aromatic guests at 25 °C.

indole, or *p*-dimethoxybenzene in $CHCl_3$ solution (Figures S2−S4, Supporting Information). For the quantitative analysis of the host−guest association in solution via CT interaction, the spectrophotometric changes were treated by the Benesi−Hildebrand procedure[22] as shown in Figure 8b, which extracted the association constants (K_{CT}) of **1** with donor guests: K_{CT} = 1.0 for α-naphthol, 0.4 for *β*-naphthol, 1.0 for indole, and 0.3 for *p*-dimethoxybenzene (Table 1). These K_{CT} values were significantly smaller than those of pyromellitic diimide-based molecular duplexes[23] and macrocycle−tweezer complexes,[14a] which suggested the CT complexes formation of an 1:1 molar ratio in the outside of the cavity of **1**. The addition of *p*-xylene to **1** in $CHCl_3$ could not provide a clear spectral change (Figure S5, Supporting Information). The HOMO and LUMO energies of **1** and electron-rich aromatic guests are also summarized in Table 1 (B3LYP/6-31G*). The observed tendency of the CT complex formation was related to the finding that the calculated HOMO energy levels of α-naphthol, *β*-naphthol, indole, and *p*-dimethoxybenezene are higher than that of **1**, whereas the HOMO energy level of *p*-xylene are lower than that of **1**.

In the case of α-naphthol, *β*-naphthol, and indole, the CT complex formation could be also monitored in the ^{1}H NMR spectral change upon the incremental addition of donor guests to the $CHCl_3$ solution of **1** (5.0×10^{-3} M). As shown in Figure 9, the addition of α-naphthol provided the subtle but distinctive upfield shifts of the signals of the pyromellitic diimide protons (H*a*) and inner benzene protons (H*c*) ($\delta\Delta$ = ca. 0.02 ppm, for 1:10 stoichiometry), whereas the shift of the benzylic (H*b*) and outer benzene protons (H*d*) were scarcely observed. This ring-current-induced complexation shifts confirmed that the pyromellitic diimide *π*-face should be in the proximity of α-naphthol *π*-face in the complexation process. Analogous complexation shifts were observed for **1** with *β*-naphthol and **1** with indole (Figure S6, Supporting Information).

In the IR spectra, the addition of 10 equiv of *β*-naphthol to the $CHCl_3$ solution of **1** (1.0×10^{-2} M) showed almost no shifts to the shorter wavenumber of the stretching vibration of the both imidecarbonyl groups of **1** and OH groups of *β*-naphthol (Figure S7, Supporting Information).[24] The results indicated that the hydrogen bonding between **1** and donor guests scarcely occurs in $CHCl_3$ even under concentrated conditions.

X-ray Crystal Structures. Since the UV/vis spectral experiments strongly suggested the formation of intermolecular CT-type complexes with **1** and the α- and *β*-naphthols, we examined their solid-state structures. Recrystallization of **1** from CH_2Cl_2 in the presence of α- or *β*-naphthol as a guest by vapor diffusion with hexane at room temperature gave yellow crystals suitable for an X-ray crystallographic analysis. The stoichiometric ratios of the **1**/α-naphthol and **1**/*β*-naphthol complexes were 1:2 and 1:1, respectively. We presumed that a coprecipitation effect along with the CT interaction served as driving force for the formation of the 1:2 **1**/α-naphthol complex in crystals because the 1:1 stoichiometric ratio was expected in $CHCl_3$ solution by the UV/vis spectral titration study. On the other hand, the stoichiometric ratio of the **1**/*β*-naphthol (1:1) in crystals corresponded to that in solution. To investigate the effect of the association ability of the guest on cocrystallization phenomena, a competitive cocrystallization experiment of **1** with α- and *β*-naphthol was examined in $CHCl_3$ solution. The composition of the clathrate was **1**/α-naphthol/*β*-naphthol (1.0:1.5:0.5) based on the ^{1}H NMR spectrum,[25] and this suggested that the guest with stronger association ability was preferentially included in the clathrate [α-naphthol (K_{CT} 1.0) and *β*-naphthol (K_{CT} 0.4)]. The hydroxyl groups of both α- and *β*-naphthols were responsible for the hydrogen bonding with the carbonyl oxygens of **1** as described below, which resulted in a 50% static disorder in the crystal.

Figure 10 shows the relative arrangement of the donor (α-naphthol) and acceptor (pyromellitic diimide moiety) of the **1**·(α-naphthol)$_2$ complex. The α-naphthol and pyromellitic diimide *π*-face are almost completely stacked, and this complete D (donor)−A (acceptor) overlap is interpreted by the efficient orbital interactions of the LUMO of the imide and the HOMO

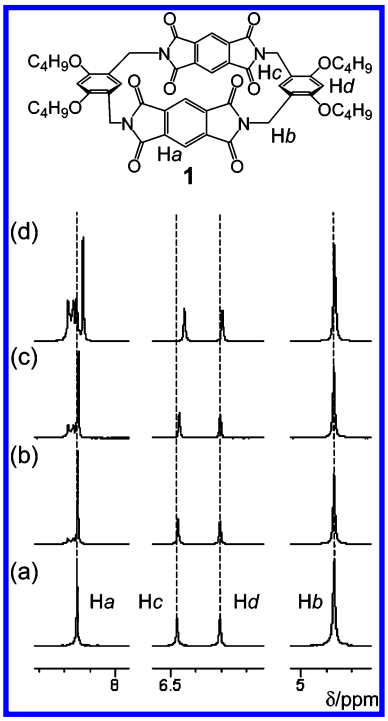

FIGURE 9. ^{1}H NMR observation of **1** recorded in $CDCl_3$ at 5×10^{-3} M (300 MHz, 25 °C, TMS as an external standard) in the presence of (a) 0, (b) 2, (c) 5, or (d) 10 equiv of α-naphthol.

(22) (a) Benesi, H. A.; Hildebrand, J. H. *J. Am. Chem. Soc.* **1949**, *71*, 2703−2707. (b) Person, W. B. *J. Am. Chem. Soc.* **1965**, *87*, 167−170.

(23) (a) Zhou, Q.-Z.; Jiang, X.-K.; Shao, X.-B.; Chen, G.-J.; Jia, M.-X.; Li, Z.-T. *Org. Lett.* **2003**, *5*, 1955−1958. (b) Zhou, Q.-Z.; Jia, M.-X.; Shao, X.-B.; Wu, L.-Z.; Jiang, X.-K.; Li, Z.-T.; Chen, G.-J. *Tetrahedron* **2005**, *61*, 7117−7124.

(24) In $CHCl_3$ solution, the OH stretching vibrations of α- and *β*-naphthol were observed at 3600 and 3324 and 3600 and 3316 cm^{-1}, respectively.[18a]

(25) The stoichiometric **1**/α-naphthol/*β*-naphthol ratio in the crystal was determined to be 1:1.5:0.5 by the ^{1}H NMR spectra (see the Experimental Section and Figure S8, Supporting Information).

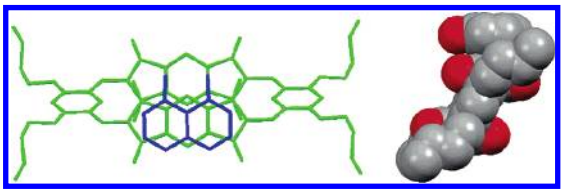

FIGURE 10. Top (left) and side (right) view of packing arrangement between **1** and α-naphthol.

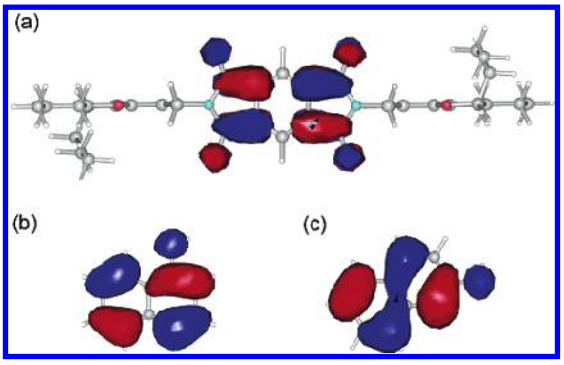

FIGURE 11. (a) LUMO orbital of **1**, (b) HOMO orbital of α-naphthol, and (c) HOMO orbital of β-naphthol calculated using B3LYP/6-31G* level of theory.

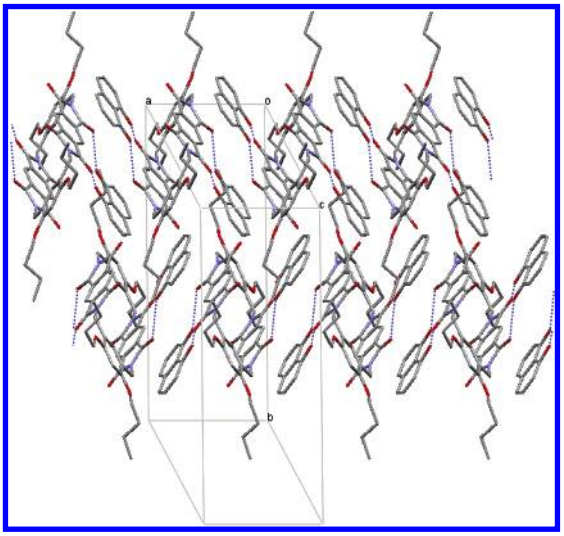

FIGURE 12. 1D molecular arrangement aligning *a*-axis via charge-transfer interaction and hydrogen bonding in **1**·(α-naphthol)$_2$. Dashed lines show hydrogen bonding. Hydrogen atoms are omitted for clarify.

of α-naphthol (Figure 11a,b). The incline of the α-naphthol π-plane and the pyromellitic diimide π-plane was only 6.0°, which revealed that the two π-planes were almost parallel. The distance between the center of the α-naphthol π-face and the pyromellitic diimide π-face, which represented the D−A distance, was 3.39 Å, supporting the presence of CT interactions between **1** and α-naphthol. Figure 12 shows the molecular packing of **1**·(α-naphthol)$_2$. In sharp contrast to the $CHCl_3$ solution, the hydrogen bonding between the carbonyl oxygens of the imide moiety of **1** and the hydroxyl groups of α-naphthol was observed with an O···O distance of 2.834(3) and 2.837(3) Å as summarized in Table 2. Clearly, the combination of the hydrogen bonding and CT interactions afforded the 1D supramolecular network aligning the *a*-axis and the 1D arrangement to form a herringbone geometry. The sandwich-like molecular arrangement of the α-naphthol·**1**·α-naphthol provided the D−A−A−D type stacking. The hydrogen bonding was also supported by the IR spectra. The cyclophane **1** exhibited asymmetric and symmetric stretching vibrations of the imidecarbonyl groups at 1777 and 1730 cm^{-1}, respectively. In **1**·(α-naphthol)$_2$, the corresponding asymmetric stretching vibration slightly shifted to 1774 cm^{-1} and the symmetric vibration was split at 1725 and 1714 cm^{-1} (Table 2). Additionally, the OH peaks of α-naphthol observed at 3324 and 3600 cm^{-1} in $CHCl_3$ but they were converged to the peak at 3443 cm^{-1} in crystals (Table 2).

Figure 13 shows the overlapping mode of β-naphthol (donor) and the pyromellitic diimide moiety (acceptor). They were stacked with the D−A distance of 3.47 Å, which was slightly longer than that of **1**·(α-naphthol)$_2$. In contrast to the complete D−A overlap in **1**·(α-naphthol)$_2$, a partial D−A overlap was observed and the overlapping mode deviated from the ideal efficient HOMO−LUMO interactions (Figure 11a,c). The incline of the β-naphthol π-plane and the pyromellitic diimide π-plane was only 7.8°. Figure 14 shows the supramolecular arrangement of the **1**·β-naphthol. Analogous to **1**·(α-naphthol)$_2$, hydrogen bonding was formed between the hydroxyl proton and the carbonyl oxygen at the imide group, with an O···O distance being 2.898(2) Å as summarized in Table 2. The hydrogen bonding was also supported by the IR spectra, which exhibited slight shifts to a shorter wavenumber of the imidecarbonyl absorptions. Similar to **1**·(α-naphthol)$_2$, the OH peaks of β-naphthol at 3316 and 3600 cm^{-1} in $CHCl_3$ converged 3462 cm^{-1} in crystals (Table 2). The hydrogen bonding in **1**·β-naphthol was almost linear with an O−H···O angle of 176°, whereas that in **1**·(α-naphthol)$_2$ was significantly bent with an O−H···O angle of 148° and 151°. It is well-known that a shorter hydrogen-bonding distance and larger O−H···O angle close to 180° are required for stronger hydrogen bonding. It is considered that the strong hydrogen bonding in the **1**·β-naphthol would induce the partial D−A overlap, and the overlapping mode was quite different from that of **1**·(α-naphthol)$_2$. The alternate arrangement of **1** and β-naphthol formed the A−A−D stacking, and repetition of this stacking mode formed a columnar arrangement aligning the *b*-axis. In addition, the hydrogen bonding between the stacked aromatic columns aligning the *a*-axis resulted in the 2D supramolecular network. These observations indicated that the cyclophane **1** could form different supramolecular assemblies depending on the positions of the hydroxyl groups of the naphthol. Thus, the pyromellitic diimide moiety included in the cyclophane framework interacted quite differently with the naphthol compared to the acyclic diimide such as *N*,*N*′-bis(2-*tert*-butylphenyl)pyromellitic diimide reported by Kishikawa and co-workers.[18a,26]

In the clathrate complexes of **1**·(α-naphthol)$_2$ and **1**·β-naphthol, slight structural changes in **1** were observed. In both **1**·(α-naphthol)$_2$ and **1**·β-naphthol, the dihedral angles between the pyromellitic diimide π-face and xylyl π-face were significantly decreased (69.0° in **1**·(α-naphthol)$_2$ and 72.5° in **1**·β-naphthol) compared to that of **1**·(DMF)$_2$ (85.4°). Furthermore, the distance of the two xylyl π-faces was 0.70 Å in **1**·β-naphthol, while the two xylyl π-faces were completely coplanar in **1**·(α-naphthol)$_2$. These observations complement the previously noted structural flexibility of **1**.

(26) It was reported that the clathrate compounds formed by *N*,*N*′-bis(2-*tert*-butylphenyl)pyromellitic diimide and phenols or indoles construct a piled sandwich-like structures in all cases.

TABLE 2. Lengths and Angles of Hydrogen Bonds and IR Peaks of the Carbonyls and OH in 1 and Clathrare Compounds

	length (Å)			angle (deg)	ν^a (cm^{-1})		
compd	O···O	O−H	H···O	O−H···O	C=O (1)	C=O (2)	O−H
1					1777	1730	
1·(α-naphthol)$_2$	2.834(3)	0.95(3)	1.98(4)	148	1774	1725, 1714	3443
	2.837(3)	0.95(3)	1.97(4)	151			
1·β-naphthol	2.898(2)	0.96(2)	1.94(2)	176	1775	1725	3462

[a] The IR spectra were measured by the KBr method.

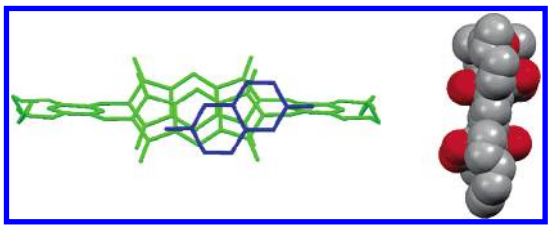

FIGURE 13. Top (left) and side (right) view of packing arrangement between **1** and β-naphthol.

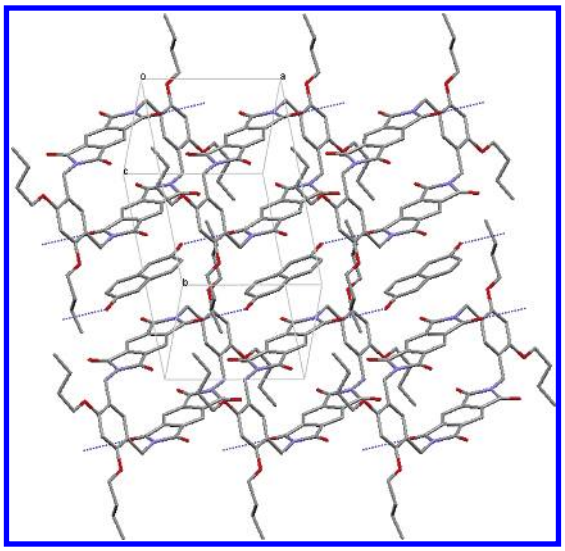

FIGURE 14. 2D molecular arrangement via charge-transfer interactions (*b*-axis) and hydrogen bonding (*a*-axis) in **1**·β-naphthol. Dashed lines show hydrogen bonding. Hydrogen atoms are omitted for clarify.

Electrochemistry. Cyclic voltammetric (CV) traces of **1** and **2** were recorded in CH_2Cl_2 solution with tetra-*n*-butylammonium hexafluorophosphate as the supporting electrolyte (Figure 15). The referential compound **2** exhibited two reversible one-electron reductions at −1.09 and −1.60 V vs Ag/Ag$^+$, and the first and second waves were ascribed to the radical anion and dianion species, respectively, based on the previously reported pyromellitic diimide derivatives (Table 3).[8e,27] Reversible redox processes were observed in both **1** and **2**. The cyclophane **1** showed the first two-electron reduction process followed by the second two-electron reduction (Figure 15). Interestingly, the first two-electron reduction wave of **1** was split into two waves at −1.01 and −1.14 V, and these waves might be ascribed to the radical anion and diradical anion species (Figure 16). Although the distance of the two pyromellitic diimide π-faces of **1** is too long to expect π-electronic interactions in the neutral species, this suggested the presence of a weak interaction between the

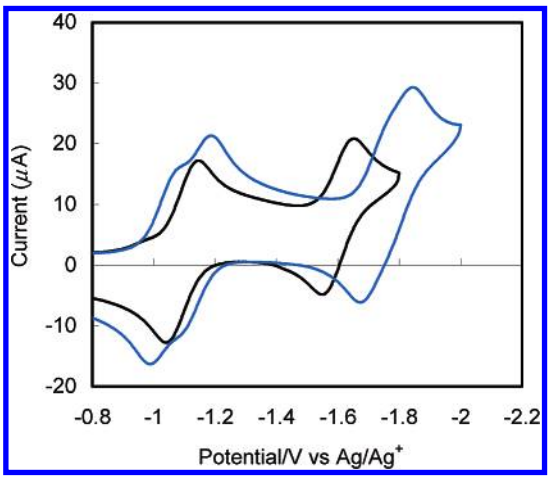

FIGURE 15. CV traces for (a) **1** (blue line) and (b) **2** (black line).

TABLE 3. Potentials (V vs Ag/Ag$^+$) for the Reduction Processes Associated with 1 and 2[a]

compd	$^1E_{1/2}$		$^2E_{1/2}$
1	−1.01	−1.14	−1.76
1 + excess α-naphthol[b]	−0.94	−1.06	
Δ*E*	+0.07	+0.08	
1 + excess β-naphthol[b]	−0.94	−1.05	
Δ*E*	+0.07	+0.09	
2	−1.09		−1.60
2 + excess α-naphthol[b]	−1.01		
Δ*E*	+0.08		
2 + excess β-naphthol[b]	−1.01		
Δ*E*	+0.08		

[a] All electrochemical measurements were performed in CH_2Cl_2 solution (5×10^{-4} M) containing 0.10 M tetra-*n*-butylammonium hexafluorophosphate at scan rate of 200 mV s^{-1}. [b] The potential was switched immediately after the first cathodic peak in the presence of 200 equiv.

radical anion and the neutral diimide moiety. Thus, the first radical anion of the one pyromellitic diimide moiety may increase the electron-density of the other diimide moiety. As a result, further one-electron reduction of the radical anion species may become harder than the first one-electron reduction. This may be one of the reasons for the observation of two distinct single-electron reduction processes for each pyromellitic diimide moiety. The second reduction processes for both pyromellitic diimide moieties were observed at the same potential (−1.76 V), which indicated that the interaction between the radical anion and the dianion hardly occurred.

Redox-dependent binding is conveniently detected by looking at the CV of the redox-active component (receptor) with and without its binding partner (substrate) present.[28] If the binding partner binds more strongly to the oxidized form of the receptor, it makes it more difficult to reduce the receptor, and half-wave potential ($E_{1/2}$) of the receptor shifts toward more negative

(27) Carroll, J. B.; Gray, M.; McMenimen, K. A.; Hamilton, D. G.; Rotello, V. M. *Org. Lett.* **2003**, *5*, 3177−3180.

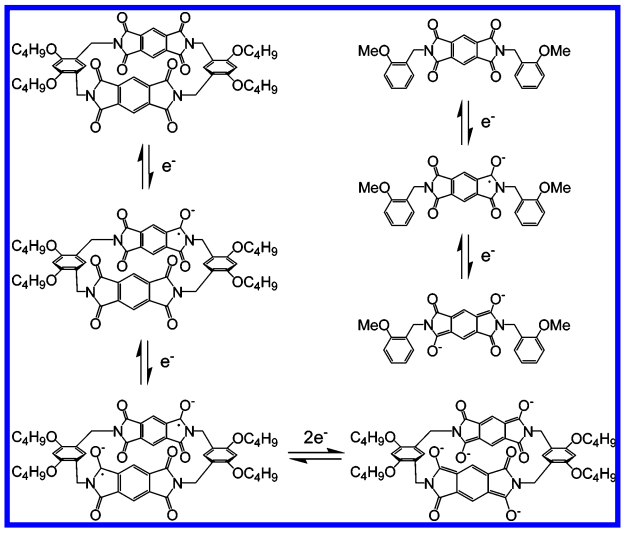

FIGURE 16. Reversible sequential reduction processes for **1** and **2**.

potentials in the presence of the substrate.[29] In contrast, if the substrate binds more strongly to the reduced form of the receptor, it will be easier to reduce the receptor in the presence of the substrate, and the $E_{1/2}$ shifts toward more positive potentials.[30]

Figure 17 shows the CV traces of **1** (diradical anion species) by itself and in the presence of α-naphthol (0.025−0.1 M). The addition of 200 equiv of α-naphthol caused the reduction to shift toward more positive potentials by ca. 80 mV with no significant change in wave height. This indicated that the diradical anion species of **1** were stabilized via noncovalent interactions between the pyromellitic diimide moiety and α-naphthol. If the potential was switched immediately after the reduction, the height of the return peak in the presence of α-naphthol remained the same as the forward peak, indicating that the diradical anion species was stable under these conditions. As summarized in Table 3, analogous positive shifts were observed for all four possible combinations of **1** and **2** with α- and *β*-naphthol. Hamilton and Rotello's group has recently reported that the dianion of the *N*,*N*′-di-*n*-butylpyromellitic diimide was stabilized in the presence of dialkylthiourea because the hydrogen bonding became strong with the increasing acceptor charge density,[27] and it was pointed out that the

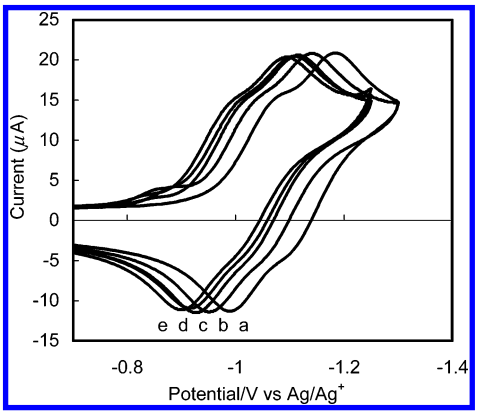

FIGURE 17. CV traces for the diradical anion of **1** in the presence of (a) 0, (b) 50, (c) 100, (d) 150, or (e) 200 equiv of α-naphthol.

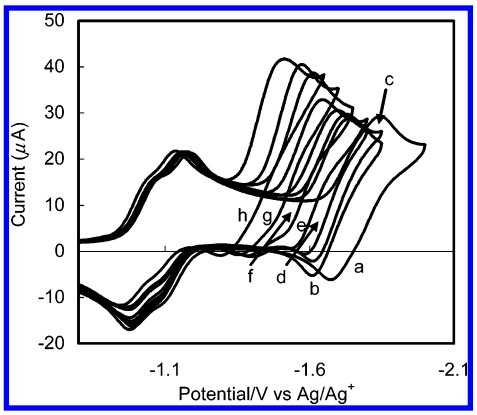

FIGURE 18. CV traces for the tetranion of **1** in the presence of (a) 0, (b) 0.5, (c) 1, (d) 2, (e) 5, (f) 10, (g) 20, or (h) 50 equiv of α-naphthol.

bifurcated hydrogen-bonding interactions was necessary for its effective stabilization according to no detectable shift in its reduction potential in the presence of excessive amounts of the trialkyl thiourea. Consequently, it is necessary to consider the pK_a value of the hydrogen bonding donor (naphthol and thiourea) in order to interpret the observations that naphthol, which is not a bifurcated hydrogen bonding donor, provided a decrease in the reduction potentials of **1** and **2**. The pK_a value (ca. 9.5) of naphthol is quite higher than that (ca. 14.5) of the thiourea derivatives, indicating that the hydroxyl group of naphthol is a strong hydrogen-bonding donor compared to the amino group of the thiourea derivatives. Considering this insight, these results indicated a reversible interaction between the di-radical anion of **1** or radical anion of **2** and naphthol. From the structural considerations, it is considered to be the reversible hydrogen bonding between the imide C═O's and the naphthol O−H's leading to the efficient stabilization of their reduced species via charge delocalization.

If the potential was scanned more negative (tetraanion in **1** and dianion in **2**) in the presence of naphthol, larger positive shifts in potential were observed for the second reduction in all four possible combinations of **1** and **2** with α- and *β*-naphthol. For example, the addition of 50 equiv of α-naphthol provided even larger positive shift in potential by ca. 360 mV for the second reduction as shown in Figure 18. Contrary to the case of the di-radical anion of **1** and radical anion of **2**, these shifts accompanied a large increase in reduction current and the lack of a return peak for the second reduction, which indicated that the irreversible multielectron processes have occurred. These

(28) For recent reviews containing aspects of supramolecular electrochemistry, see: (a) Boulas, P. L.; Gómez-Kaifer, M.; Echegoyen, L. *Angew. Chem., Int. Ed.* **1998**, *37*, 216−247. (b) Niemz, A.; Rotello, V. M. *Acc. Chem. Res.* **1999**, *32*, 44−52. (c) Kaifer, A. E. *Acc. Chem. Res.* **1999**, *32*, 62−71. (d) Tucker, J. H. R.; Collinson, S. R. *Chem. Soc. Rev.* **2002**, *31*, 147−156. (e) Cooke, G.; Rotello, V. M. *Chem. Soc. Rev.* **2002**, *31*, 275−286.

(29) For hydrogen-bonded host−guest complexes with binding efficiencies that increase upon electrochemical oxidation, see: (a) Carr, J. D.; Lambert, L.; Hibbs, D. E.; Hursthouse, M. B.; Malik, K. M. A.; Tucker, J. H. R. *Chem. Commun.* **1997**, 1649−1650. (b) Carr, J. D.; Coles, S. J.; Hursthouse, M. B.; Light, M. E.; Tucker, J. H. R.; Westwood, J. *Angew. Chem., Int. Ed.* **2000**, *39*, 3296−3299. (c) Collinson, S. R.; Gelbrich, T.; Hursthouse, M. B.; Tucker, J. H. R. *Chem. Commun.* **2001**, 555−556. (d) Bourgel, C.; Boyd, A. S. F.; Cooke, G.; de Cremiers, H. A.; Duclairoir, F. M. A.; Rottello, V. M. *Chem. Commun.* **2001**, 1954−1955.

(30) For hydrogen-bonded host−guest complexes with binding efficiencies that increase upon electrochemical reduction, see: (a) Ge, Y.; Lilienthal, R. R.; Smith, D. K. *J. Am. Chem. Soc.* **1996**, *118*, 3976−3977. (b) Ge, Y.; Miller, L.; Ouimet, T.; Smith, D. K. *J. Org. Chem.* **2000**, *65*, 8831−8838. (c) Bu, J.; Lilienthal, N. D.; Woods, J. E.; Nohrden, C. E.; Hoang, K.-P. T.; Truong, D.; Smith, D. K. *J. Am. Chem. Soc.* **2005**, *127*, 6423−6429. (d) Chan-Leonor, C.; Martin, S. L.; Smith, D. K. *J. Org. Chem.* **2005**, *70*, 10817−10822.

phenomena may be responsible for proton transfer from naphthol to the more basic tetraanion of **1** or dianion of **2**, quite possibly facilitated by the hydrogen bonding as is the case with the diarylurea/dinitrobenzene^{2-} (2:1) system.[30d]

3. Conclusions

In conclusion, we have demonstrated that the newly synthesized [2 + 2] pyromellitic diimide-based cyclophane **1** constructed 1D and 2D supramolecular assemblies and exhibited redox modulation via noncovalent interactions with naphthols. A combination of the CT interactions and hydrogen bonding led to the formation of clathrate compounds with the regioselectivity of the hydroxyl group of naphthol, which resulted in the 1D network in the clathrate of **1** and α-naphthol in an 1:2 ratio, and the 2D network in the clathrate of **1** and *β*-naphthol in an 1:1 ratio. Our approach is an example of creating a supramolecular assembly in the solid state using both the CT interaction and hydrogen bonding in the outside of the cavity of the cyclophane host **1**. Upon the addition with naphthol, the first two-electron reduction potential ascribed to the di-radical anion of **1** and the radical anion of **2** are moderately decreased due to the formation of reversible hydrogen bonding with an increasing charge density of the acceptor.

In UV/vis spectroscopy, a very weak intramolecular CT interaction was observed between the pyromellitic diimide moiety and the alkoxy-substituted benzene moiety of **1** and **2**. This is attributed to the introduction of a methylene linker between them, which could not decrease the electron-withdrawing property of the pyromellitic diimide moiety to form the observed supramolecular assemblies in the solid states. In the cyclic voltammetry measurements, two different reduction potentials in **1** were observed for the first two-electron reduction, and this may be ascribed to the stepwise reduction of the neutral species to the radical anion, followed by a further reduction to the dianion species.

We expect that the cyclophane **1**, which has not only a fully structural flexibility but also parallel arrangement of the transannular pyromellitic diimide *π*-faces, is a candidate as a structural component for the construction of a new covalent organic nanotube[31] with an extended 1D *π*-system because an additional structural modification of **1** may be possible at the 3- and 6-positions of its pyromellitic diimide moieties. Our synthetic study of the covalent organic nanotubes utilizing a pyromellitic diimide-based cyclophane structure is now in progress, and the results will be reported elsewhere. We believe that the present study provides valuable information for the creation of new pyromellitic diimide-based supramolecular structures.

4. Experimental Section

[2 + 2] Pyromellitic Diimide-Based Cyclophane (1). A solution of 1,3-bis(aminomethyl)-4,6-di-*n*-butoxybenzene **7** (1.45 g, 5.26 mmol) in dry THF (200 mL) and a solution of pyromellitic dianhydride **8** (1.15 g, 5.26 mmol) in dry THF (200 mL) were simultaneously added to dry THF (100 mL) at 60 °C over a period of 7 h with stirring under an argon atmosphere. After the addition, the reaction mixture was stirred at 60 °C for 12 h, and the reaction mixture was evaporated in vacuo to dryness to give the amic acid. In the ^{1}H NMR spectra, the broad COOH signals of the intermediate amic acid derivatives were observed at around 13−14 ppm in DMSO-d_6 solution. A solution of the amic acid and NaOAc (431 mg, 5.26 mmol) in Ac_2O (60 mL) was heated at 110 °C for 4 h. The reaction mixture was poured into water (400 mL), and the precipitate was collected by filtration. The precipitate was dissolved in $CHCl_3$ (500 mL), insoluble material was removed by filtration, and the filtrate was evaporated in vacuo to dryness. The residue was purified by silica gel column chromatography eluting with $CHCl_3$ to give **1** in 24% yield (583 mg, 0.63 mmol) as a pale green powder: mp > 300 °C; IR (KBr) ν_{max} 2957, 1777, 1730 ($\nu_{C=O}$), 1621, 1510, 1383, 1307, 1187 cm^{-1}; ^{1}H NMR (300 MHz, $CDCl_3$) δ 1.01 (t, J = 7.3 Hz, 12 H, CH_3), 1.52−1.62 (m, 8 H, CH_2), 1.84 (tt, J = 6.2 Hz, 8 H, CH_2), 4.04 (t, J = 6.2 Hz, 8 H, OCH_2), 4.87 (s, 8 H, benzyl H), 6.30 (s, 2 H, ArH), 6.48 (s, 2 H, ArH) 8.15 (s, 4 H, ArH); FAB-MS (NBA, positive) 925 [(M + H)$^+$]. Anal. Calcd for $C_{52}H_{52}N_4O_{12}$: C, 67.52; H, 5.67; N, 6.06. Found: C, 67.27; H, 5.69; N, 6.09.

***N,N′*-Bis(2-methoxybenzyl)pyromellitic Diimide (2).** To a solution of the anhydride **8** (1.00 g, 4.59 mmol) in dry THF (20 mL) was added a dry THF solution (10 mL) of 2-methoxybenzylamine **9** (1.38 g, 10.1 mmol) with stirring at room temperature under an argon atmosphere. After the mixture was stirred at 60 °C for 12 h, the reaction mixture was evaporated in vacuo to dryness to give the amic acid. A solution of the amic acid and NaOAc (346 mg, 4.59 mmol) in Ac_2O was heated at 110 °C for 4 h, the reaction mixture was poured into water (300 mL), and the precipitate was collected by filtration. The precipitate was dissolved in $CHCl_3$ (300 mL), and insoluble material was removed by filtration. The residue was purified by silica gel column chromatography eluting with $CHCl_3$/AcOEt (20:1, v/v) and recrystallized from $CHCl_3$ to give **2** in 72% yield (1.51 g, 3.30 mmol) as a pale green powder: mp 283−284 °C; IR (KBr) ν_{max} 1773, 1710 ($\nu_{C=O}$), 1495, 1464, 1444, 1393, 1343, 1273, 1250, 1107, 1032 cm^{-1}; ^{1}H NMR (300 MHz, CD_2Cl_2) δ 3.82 (s, 6 H, OCH_3), 4.10 (s, 4 H, benzyl H), 6.89 (td, J = 1.2, 7.2 Hz, 2 H, ArH), 6.90 (dd, J = 1.2, 7.2 Hz, 2 H, ArH), 7.19 (dd, J = 1.7, 7.6 Hz, 2 H, ArH), 7.28 (dd, J = 1.7, 7.6 Hz, 2 H, ArH); FAB-MS (NBA, positive) 457 [(M + H)$^+$]. Anal. Calcd for $C_{26}H_{20}N_2O_6$: C, 68.42; H, 4.42; N, 6.14. Found: C, 68.17; H, 4.39; N, 6.11.

1,3-Bis(aminomethyl)-4,6-di-*n*-butoxybenzene (7). Preparation of this compound has been already reported,[19] but we describe a modified high-yield procedure here. To a solution of the dinitrile **6** (817 mg, 3.00 mmol) in dry toluene (5 mL) was added 1.5 M diisobutylaluminum hydride solution (20.0 mL, 30.0 mmol) at room temperature under an argon atmosphere. After the mixture was heated at 110 °C for 4 h, the reaction mixture was poured into ice−water (50 mL). Aqueous NaOH solution (1 N, 10 mL) was added, and the mixture was extracted with Et_2O (30 mL × 3). The combined organic layers were washed with brine, dried with Na_2SO_4, and evaporated in vacuo to dryness to give 1,3-bis(aminomethyl)-4,6-di-*n*-butoxybenzene **7** in 81% yield (667 mg, 2.42 mmol) as colorless oil whose ^{1}H NMR data are in complete agreement with those in the literature:[19] ^{1}H NMR (300 MHz, $CDCl_3$) δ 0.99 (t, J = 7.3 Hz, 6 H, CH_3), 1.44−1.58 (m, 4 H, CH_2), 1.74−1.84 (m, 4 H, CH_2), 3.74 (s, 4 H, benzyl H), 3.98 (t, J = 6.3 Hz, 4 H, OCH_2), 6.42 (s, 1 H, ArH), 7.05 (s, 1 H, ArH).

Determination of Association Constants (K_{CT}). In the presence of a large excess of electron-rich aromatic guests, K_{CT} values of the CT complexes were determined in $CHCl_3$ by a spectrophotometric procedure based on the Benesi−Hildebrand relationship[22] at 25 °C. In all cases, linear correlations were observed, indicating an 1:1 molar ratio for the CT complexes. From the linear plot of Δabsorbance^{-1} against [guest]$^{-1}$, consisting of at least eight data

(31) For covalent organic nanotubes, see: (a) Harada, A.; Li, J.; Kamachi, M. *Nature* **1993**, *364*, 516−518. (b) Ikeda, A.; Shinkai, S. *Chem. Commun.* **1994**, 2375−2376. (c) Pérez-Adelmar, J.-A.; Abraham, H.; Sánchez, C.; Rissanen, K.; Prados, P.; de Mendoza, J. *Angew. Chem., Int. Ed. Engl.* **1996**, *35*, 1009−1011. (d) Kim, S. K.; Sim, W.; Vicens, J.; Kim, J. S. *Tetrahedron Lett.* **2003**, *44*, 805−809. (e) Kim, S. K.; Vicens, J.; Park, K.-M.; Lee, S. S.; Kim, J. S. *Tetrahedron Lett.* **2003**, *44*, 993−997. (f) Kim, Y.; Mayer, M. F.; Zimmerman, S. C. *Angew. Chem., Int. Ed.* **2003**, *42*, 1121−1126. (g) Organo, V. G.; Leontiev, A. V.; Sgarlata, V.; Dias, H. V. R.; Rudkevich, D. M. *Angew. Chem., Int. Ed.* **2005**, *44*, 3043−3047. (h) Jin, W.; Fukushima, T.; Kosaka, A.; Niki, M.; Ishii, N.; Aida, T. *J. Am. Chem. Soc.* **2005**, *127*, 8284−8285.

points, the slope was estimated as $(K_{CT}\epsilon_{CT})^{-1}$ and the intercept as $(\epsilon_{CT})^{-1}$. Linear fits obtained by the least-squares method had a correlation coefficient of > 0.999.

Preparation of the Charge-Transfer Complexes. General procedure for the preparation of **1**·(α-naphthol)$_2$ and **1**·*β*-naphthol: Recrystallization of **1** (7.0 mg, 7.6×10^{-3} *μ*mol) from the CH_2Cl_2 solution (2 mL) in the presence of α-naphthol (3.3 mg, 2.3×10^{-2} *μ*mol) by vapor diffusion with hexane (6 mL) at room temperature gave yellow crystals on standing for 1 d. The resultant crystals were collected by decantation from the solvent.

Competitive cocrystallization experiment: Recrystallization of **1** (7.0 mg, 7.6×10^{-3} *μ*mol) from the CH_2Cl_2 solution (2 mL) in the presence of α-naphthol (2.2 mg, 1.5×10^{-2} *μ*mol) and *β*-naphthol (2.2 mg, 1.5×10^{-2} *μ*mol) by vapor diffusion with hexane (6 mL) at room temperature gave yellow crystals on standing for 1 d. The resultant crystals were collected by decantation from the solvent and determined to be **1**/α-naphthol/*β*-naphthol (1:1.5:0.5) complex based on the comparison between the integral intensity in the ^{1}H NMR spectrum of **1**/α-naphthol/*β*-naphthol complex, **1** (1×10^{-2} M) in the presence of α-naphthol (2×10^{-2} M), and **1** (1×10^{-2} M) in the presence of *β*-naphthol (2×10^{-2} M) (Figure S8, Supporting Information).

X-ray Crystallographic Structural Analysis. Data are summarized in the Supporting Information.

Theoretical Methods. All calculations were performed using the Gaussian 03[32] suite of programs. Optimized structure, frequency calculations, and single-point energy calculations were performed using the Becke's three-parameter hybrid functional (B3)[33] with the correlation functional of Lee, Yang, and Parr (LYP),[34,35] and the basis sets 6-31G*. Restricted calculations were performed, as all relevant species were closed shell molecules. All reported energies include zero-point energy.

Acknowledgment. S.K. is grateful for the partial financial support by the Sasakawa Scientific Research Grant from The Japan Science Society. We gratefully acknowledge the financial support by the Theme Project of Molecular Architecture of Organic Compounds for Functional Design (Professor Tahsin J. Chow), Institute of Chemistry, Academia Sinica, Taiwan, R.O.C. We are also grateful for partial financial support by the Joint Project of Chemical Synthesis Core Research Institutions, Research and Education for Inter-University Research Project, MEXT, Japan. We thank Professor Shuntaro Mataka and Dr. Tsutomu Ishi-i (Kyushu University) for the cyclic voltammetry measurements and Professor Masaaki Mishima (Kyushu University) for the MO calculations.

Supporting Information Available: Temperature-dependent ^{1}H NMR spectra of **1** (Figure S1), UV/vis spectra of **1** and **1** plus *β*-naphthol (Figure S2), UV/vis spectra of **1** and **1** plus indole (Figure S3), UV/vis spectra of **1** and **1** plus *p*-dimethoxybenzene (Figure S4), UV/vis spectra of **1** and **1** plus *p*-xylene (Figure S5), ^{1}H NMR observations of **1** recorded in $CDCl_3$ in the presence of *β*-naphthol and indole (Figure S6), IR spectra of **1** plus *β*-naphthol in $CHCl_3$ (Figure S7), ORTEP drawings for **1** and α-naphthol (Figure S8), ORTEP drawings for **1** and *β*-naphthol (Figure S9), CV traces for **1** in the presence of *β*-naphthol (Figure S10), CV traces for **2** in the presence of α-naphthol (Figure S11), CV traces for **2** in the presence of *β*-naphthol (Figure S12), calculated coordinates and/or total energies of optimized *syn*-**1′** (Table S1), *anti*-**1′** (Table S2), *parallel*-**1′** (Table S3), **1** (Table S4), and **2** (Table S5), and structural data for the X-ray analyses (positional and thermal parameters, bond distances and angles in CIF format) of **1**·(DMF)$_2$, **1**·(α-naphthol)$_2$, and **1**·*β*-naphthol. This material is available free of charge via the Internet at http://pubs.acs.org.

JO0600196

(32) Frisch, M. J.; Trucks, G. W.; Schlegel, H. B.; Scuseria, G. E.; Robb, M. A.; Cheeseman, J. R.; Montgomery, J. A., Jr.; Vreven, T.; Kudin, K. N.; Burant, J. C.; Millam, J. M.; Iyengar, S. S.; Tomasi, J.; Barone, V.; Mennucci, B.; Cossi, M.; Scalmani, G.; Rega, N.; Petersson, G. A.; Nakatsuji, H.; Hada, M.; Ehara, M.; Toyota, K.; Fukuda, R.; Hasegawa, J.; Ishida, M.; Nakajima, T.; Honda, Y.; Kitao, O.; Nakai, H.; Klene, M.; Li, X.; Knox, J. E.; Hratchian, H. P.; Cross, J. B.; Bakken, V.; Adamo, C.; Jaramillo, J.; Gomperts, R.; Stratmann, R. E.; Yazyev, O.; Austin, A. J.; Cammi, R.; Pomelli, C.; Ochterski, J. W.; Ayala, P. Y.; Morokuma, K.; Voth, G. A.; Salvador, P.; Dannenberg, J. J.; Zakrzewski, V. G.; Dapprich, S.; Daniels, A. D.; Strain, M. C.; Farkas, O.; Malick, D. K.; Rabuck, A. D.; Raghavachari, K.; Foresman, J. B.; Ortiz, J. V.; Cui, Q.; Baboul, A. G.; Clifford, S.; Cioslowski, J.; Stefanov, B. B.; Liu, G.; Liashenko, A.; Piskorz, P.; Komaromi, I.; Martin, R. L.; Fox, D. J.; Keith, T.; Al-Laham, M. A.; Peng, C. Y.; Nanayakkara, A.; Challacombe, M.; Gill, P. M. W.; Johnson, B.; Chen, W.; Wong, M. W.; Gonzalez, C.; Pople, J. A. Gaussian 03, revision C.02; Gaussian, Inc.: Wallingford, CT, 2004.

(33) Becke, A. D. *J. Chem. Phys.* **1993**, *98*, 5648−5652.

(34) Lee, C.; Yang, W.; Parr, R. G. *Phys. Rev. B* **1988**, *37*, 785−789.

(35) Miehlich, B.; Savin, A.; Stoll, H.; Preuss, H. *Chem. Phys. Lett.* **1989**, *157*, 200−206.